


Phase diagram of the J_1 - J_2 quantum Heisenberg model for arbitrary spin

Andreas Rückriegel, Dmytro Tarasevych , and Peter Kopietz

Institut für Theoretische Physik, Universität Frankfurt, Max-von-Laue Straße 1, 60438 Frankfurt, Germany



(Received 22 March 2024; revised 18 April 2024; accepted 22 April 2024; published 6 May 2024)

We use the spin functional renormalization group to investigate the J_1 - J_2 quantum Heisenberg model on a square lattice. By incorporating sum rules associated with the fixed length of the spin operators as well as the nontrivial quantum dynamics implied by the spin algebra, we are able to compute the ground state phase diagram for arbitrary spin S , including the quantum paramagnetic phase at strong frustration. Our prediction for the extent of this paramagnetic region for $S = 1/2$ agrees well with other approaches that are computationally more expensive. We find that the quantum paramagnetic phase disappears for $S \gtrsim 5$ due to the suppression of quantum fluctuations with increasing S .

DOI: [10.1103/PhysRevB.109.184410](https://doi.org/10.1103/PhysRevB.109.184410)

I. INTRODUCTION

One of the major challenges in contemporary condensed matter physics is the calculation of ground state properties of frustrated spin systems [1–5]. In these systems, quantum fluctuations play a dominant role at low temperatures and may even be strong enough to melt any classical long-range order. This results in novel, highly entangled quantum paramagnetic ground states like spin liquids or resonating valence bond states. Due to the absence of classical magnetic order, such quantum paramagnets cannot be investigated using standard approaches to quantum spin systems such as spin-wave theory. At the same time, sign problems prevent large-scale unbiased quantum Monte Carlo simulations for frustrated spin systems [2]. While the density-matrix renormalization group [6,7] offers an efficient means of determining ground state properties of strongly correlated systems in reduced dimensions, its computational complexity increases drastically with system size in higher dimensions because of area-law entanglement growth. Therefore there is a need to develop unbiased methods to address frustrated spin systems in arbitrary dimensions. One such method is the functional renormalization group (FRG) [8–13]. In a seminal work by Reuther and Wölfle [14], the established machinery of FRG for electronic systems was applied to a frustrated quantum spin system by representing the spin operators in terms of auxiliary fermions. Since then, this so-called pseudofermion FRG has been used as an unbiased numerical tool to study a variety of frustrated quantum spin systems in two and three dimensions; for a recent review, see Ref. [15] and references therein. However, because of the mapping to auxiliary fermions, this approach suffers from several disadvantages. For example, the Hilbert space of the fermions contains unphysical states which may contaminate physical results. This problem has been addressed recently by using either a pseudo-Majorana fermion representation of the spin operators [16–19] or implementing the so-called Popov-Fedotov trick [20,21]. Moreover, since a spin operator is represented by two fermionic operators, computing n -spin correlation functions requires $2n$ -fermion correlation functions. This makes it difficult to include correlations

involving more than two spins. Finally, because of the nontrivial spin dynamics, obtaining explicit solutions necessitates heavy numerical computations even for modest truncations of the FRG flow equations. An alternative FRG approach to quantum spin systems is the spin FRG, proposed by Krieg and Kopietz [22], and further developed in Refs. [23–29]. It relies on a formally exact renormalization group flow equation for the generating functional of the physical spin correlation functions, without the need to introduce auxiliary boson or fermion operators and their associated subtleties and restrictions.

In our recent work [29], we have demonstrated that even simple truncations of the spin FRG flow already yield quantitatively accurate results for classical, finite temperature phase transitions in quantum spin systems, for arbitrary spin S . Here, we extend this approach to quantum phase transitions in frustrated spin systems and demonstrate that the spin FRG is a powerful yet computationally rather cheap method to study the zero-temperature phase diagram of quantum paramagnets. To that end, we consider a paradigmatic model system for a frustrated quantum magnet: the antiferromagnetic J_1 - J_2 model with Hamiltonian

$$\mathcal{H} = J_1 \sum_{\langle ij \rangle_1} \mathbf{S}_i \cdot \mathbf{S}_j + J_2 \sum_{\langle ij \rangle_2} \mathbf{S}_i \cdot \mathbf{S}_j \quad (1)$$

on the square lattice, where $J_1, J_2 \geq 0$ are antiferromagnetic exchange couplings, the spin- S operators \mathbf{S}_i satisfy $\mathbf{S}_i^2 = S(S+1)$, and $\langle ij \rangle_{1(2)}$ denotes all pairs of nearest (next-nearest) neighbors. The Fourier transform of the exchange interaction is then

$$J(\mathbf{k}) = 4J_1\gamma_1(\mathbf{k}) + 4J_2\gamma_2(\mathbf{k}), \quad (2)$$

with the nearest and next-nearest neighbor form factors,

$$\gamma_1(\mathbf{k}) = \frac{1}{2}(\cos k^x + \cos k^y), \quad (3a)$$

$$\gamma_2(\mathbf{k}) = \cos k^x \cos k^y, \quad (3b)$$

where wave vectors are measured in units of the inverse lattice spacing. This model represents one of the simplest quantum spin systems where one can study how frustration induces large quantum fluctuations that destroy classical

order. As such, it has been intensively studied in the last decades using a variety of methods, ranging from spin-wave theory [30–32] and Green’s function methods [33–36] over large- N expansion [37], an effective nonlinear σ model [38], Schwinger-boson mean field theory [39], bond operators [40–43], series expansions [44–47], exact diagonalization [48–50] density matrix renormalization group [51–55], Monte Carlo [50,51], coupled cluster simulations [56], hierarchical mean-field theory [57], variational approaches [58–63], pseudofermion FRG [14], as well as neural networks [64]. Apart from the spin-wave calculations, all of these works focus on the $S = 1/2$ case, where quantum effects are most pronounced. The consensus from these studies on the phase diagram for $S = 1/2$ is as follows: For weak next-nearest neighbor coupling, $J_2 \lesssim 0.4J_1$, the system exhibits two-sublattice Néel order, with ordering wave vector $\mathbf{Q} = (\pi, \pi)$. In the opposite limit of strong next-nearest neighbor coupling, $J_2 \gtrsim 0.65J_1$, the system orders into a stripe state with ordering wave vector either $\mathbf{Q} = (\pi, 0)$ or $(0, \pi)$. In the intermediate, strongly frustrated range of exchange couplings, the ground state is a quantum paramagnet. The exact nature of this paramagnetic phase, as well as of the phase transition into it, is still under debate [37,40,42,44,46,49,51–55,57,58,62,64]. It is also not certain [2] whether this exotic phase survives for $S > 1/2$, as indicated by spin wave theory [30]. As quantum fluctuations decrease with increasing S , the paramagnetic phase must eventually disappear for large spin and give way to a first order transition from Néel to the stripe state at $J_2 = 0.5J_1$ as in the classical system at $S \rightarrow \infty$. In this work, we use the spin FRG to compute the ground state phase diagram of the J_1 - J_2 model for arbitrary spin S and thereby show that the paramagnetic phase disappears for spin $S \gtrsim 5$.

The rest of this paper is organized as follows. In Sec. II, we introduce the basic idea of spin FRG and present the relevant flow equations. We also discuss how the spin algebra entails both an infinite tower of sum rules for the spin vertices and nontrivial dynamics, both of which are crucial to develop a nonperturbative truncation scheme of the FRG flow equations which allows us to detect possible quantum phase transitions. The resulting truncated system of flow equations is then solved numerically in Sec. III to obtain the phase diagram of the J_1 - J_2 model. In the final Sec. IV, we summarize our main results and discuss how it could be extended in future work. Additional technical details are presented in three appendices. In Appendix A, we explain in detail how the spin FRG flow equations are rescaled such that the flow directly generates the temperature dependence of spin correlation functions. Appendix B shows how the operator identity $S_i^2 = S(S + 1)$ implies an infinite tower of sum rules for the spin

vertices which can be elegantly derived from the spin FRG flow equations. Finally, in Appendix C, we derive the high-frequency approximation of the truncated flow equations.

II. NONPERTURBATIVE TRUNCATION OF FRG FLOW EQUATIONS

A. Vertex expansion and exact flow equations

To implement the spin FRG, we continuously deform the exchange interaction $J(\mathbf{k}) \rightarrow J_\Lambda(\mathbf{k})$ with a scale $\Lambda \in [0, 1]$, such that $J_{\Lambda=0}(\mathbf{k}) = 0$ and $J_{\Lambda=1}(\mathbf{k}) = J(\mathbf{k})$. At the initial scale $\Lambda = 0$, the system then decouples into an ensemble of isolated quantum spins, for which one can compute arbitrary correlation functions analytically [24,65–67]. The evolution from this initial condition to the full interacting Heisenberg model (1) with increasing Λ is then described by the spin FRG flow equations. In this work, we use a simple multiplicative deformation scheme that linearly switches on the exchange interaction [22,29],

$$J_\Lambda(\mathbf{k}) = \Lambda J(\mathbf{k}). \quad (4)$$

In the absence of external magnetic fields, this deformation scheme merely multiplies the Heisenberg model (1) by the deformation parameter Λ . Thus it can also be interpreted as changing the temperature T to T/Λ . In effect, the Λ flow is therefore equivalent to a temperature flow [68] that starts at $T \rightarrow \infty$ ($\Lambda = 0$) and ends at the physical temperature T ($\Lambda = 1$). This allows one to extract the full temperature dependence of the spin correlation functions from a single solution of the FRG flow equations, as explained in more detail in Appendix A. In this way, one can see that the spin FRG flow equations are perturbatively controlled in $J(\mathbf{k})/T$. An iterative solution of the flow equations consequently generates the high-temperature expansion. The goal of the spin FRG formalism can thus be understood as an attempt to extrapolate from the perturbatively controlled high-temperature regime to low temperatures by re-summing certain classes of diagrams.

Because at the initial scale $\Lambda = 0$ each individual spin is conserved, special care has to be taken in defining suitable vertex functions for the dynamic part of the spin fluctuations [22,24,26]. Here, we employ the “hybrid vertices” introduced in Ref. [26] that are one-line irreducible only in the static sector, and interaction-irreducible in the dynamic sector. Their generating functional $\Gamma_\Lambda[\mathbf{m}, \boldsymbol{\eta}]$ then depends both on the static (classical) magnetization \mathbf{m} as well as on a dynamic (quantum) auxiliary field $\boldsymbol{\eta}$. The latter can be interpreted as the dynamic part of a fluctuating exchange field. In the paramagnetic phase of our spin-rotation invariant Heisenberg model defined in Eq. (1), this generating functional has the vertex expansion

$$\begin{aligned} \Gamma_\Lambda[\mathbf{m}, \boldsymbol{\eta}] &= N f_\Lambda/T + \frac{1}{2T} \int_{\mathbf{k}} [J(\mathbf{k}) + \Sigma_\Lambda(\mathbf{k})] \mathbf{m}_{\mathbf{k}} \cdot \mathbf{m}_{-\mathbf{k}} - \frac{1}{2} \int_{\mathbf{K}} [G(\mathbf{k}) + \Pi_\Lambda(\mathbf{K})] \boldsymbol{\eta}_{\mathbf{K}} \cdot \boldsymbol{\eta}_{-\mathbf{K}} \\ &+ \frac{1}{2} \int_{\mathbf{k}_1} \int_{\mathbf{K}_2} \int_{\mathbf{K}_3} \delta(\mathbf{k}_1 + \mathbf{K}_2 + \mathbf{K}_3) \Gamma_\Lambda^{\mathbf{x}\bar{\mathbf{y}}\bar{\mathbf{z}}}(\mathbf{k}_1, \mathbf{K}_2, \mathbf{K}_3) \mathbf{m}_{\mathbf{k}_1} \cdot (\boldsymbol{\eta}_{\mathbf{K}_2} \times \boldsymbol{\eta}_{\mathbf{K}_3}) \\ &+ \frac{1}{3!} \int_{\mathbf{K}_1} \int_{\mathbf{K}_2} \int_{\mathbf{K}_3} \delta(\mathbf{K}_1 + \mathbf{K}_2 + \mathbf{K}_3) \Gamma_\Lambda^{\bar{\mathbf{x}}\bar{\mathbf{y}}\bar{\mathbf{z}}}(\mathbf{K}_1, \mathbf{K}_2, \mathbf{K}_3) \boldsymbol{\eta}_{\mathbf{K}_1} \cdot (\boldsymbol{\eta}_{\mathbf{K}_2} \times \boldsymbol{\eta}_{\mathbf{K}_3}) \end{aligned}$$

$$\begin{aligned}
 & + \frac{1}{4!T} \int_{\mathbf{k}_1} \int_{\mathbf{k}_2} \int_{\mathbf{k}_3} \int_{\mathbf{k}_4} \delta(\mathbf{k}_1 + \mathbf{k}_2 + \mathbf{k}_3 + \mathbf{k}_4) \sum_{\alpha_1 \dots \alpha_4} \Gamma_{\Lambda}^{\alpha_1 \alpha_2 \alpha_3 \alpha_4}(\mathbf{k}_1, \mathbf{k}_2, \mathbf{k}_3, \mathbf{k}_4) m_{\mathbf{k}_1}^{\alpha_1} m_{\mathbf{k}_2}^{\alpha_2} m_{\mathbf{k}_3}^{\alpha_3} m_{\mathbf{k}_4}^{\alpha_4} \\
 & + \frac{1}{(2!)^2} \int_{\mathbf{k}_1} \int_{\mathbf{k}_2} \int_{\mathbf{K}_3} \int_{\mathbf{K}_4} \delta(\mathbf{k}_1 + \mathbf{k}_2 + \mathbf{K}_3 + \mathbf{K}_4) \sum_{\alpha_1 \dots \alpha_4} \Gamma_{\Lambda}^{\alpha_1 \alpha_2 \tilde{\alpha}_3 \tilde{\alpha}_4}(\mathbf{k}_1, \mathbf{k}_2, \mathbf{K}_3, \mathbf{K}_4) m_{\mathbf{k}_1}^{\alpha_1} m_{\mathbf{k}_2}^{\alpha_2} \eta_{\mathbf{K}_3}^{\alpha_3} \eta_{\mathbf{K}_4}^{\alpha_4} \\
 & + \frac{1}{3!} \int_{\mathbf{k}_1} \int_{\mathbf{K}_2} \int_{\mathbf{K}_3} \int_{\mathbf{K}_4} \delta(\mathbf{k}_1 + \mathbf{K}_2 + \mathbf{K}_3 + \mathbf{K}_4) \sum_{\alpha_1 \dots \alpha_4} \Gamma_{\Lambda}^{\alpha_1 \tilde{\alpha}_2 \tilde{\alpha}_3 \tilde{\alpha}_4}(\mathbf{k}_1, \mathbf{K}_2, \mathbf{K}_3, \mathbf{K}_4) m_{\mathbf{k}_1}^{\alpha_1} \eta_{\mathbf{K}_2}^{\alpha_2} \eta_{\mathbf{K}_3}^{\alpha_3} \eta_{\mathbf{K}_4}^{\alpha_4} \\
 & + \frac{1}{4!} \int_{\mathbf{K}_1} \int_{\mathbf{K}_2} \int_{\mathbf{K}_3} \int_{\mathbf{K}_4} \delta(\mathbf{K}_1 + \mathbf{K}_2 + \mathbf{K}_3 + \mathbf{K}_4) \sum_{\alpha_1 \dots \alpha_4} \Gamma_{\Lambda}^{\tilde{\alpha}_1 \tilde{\alpha}_2 \tilde{\alpha}_3 \tilde{\alpha}_4}(\mathbf{K}_1, \mathbf{K}_2, \mathbf{K}_3, \mathbf{K}_4) \eta_{\mathbf{K}_1}^{\alpha_1} \eta_{\mathbf{K}_2}^{\alpha_2} \eta_{\mathbf{K}_3}^{\alpha_3} \eta_{\mathbf{K}_4}^{\alpha_4} + \dots \quad (5)
 \end{aligned}$$

Here, f_{Λ} is the scale-dependent free energy density, the dots stand for terms with more than four fields, and $K = (\mathbf{k}, \omega)$ collects wave vectors \mathbf{k} and Matsubara frequencies ω . The associated integration and delta symbols are $\int_K = T \sum_{\omega} \int_{\mathbf{k}} = (T/N) \sum_{\mathbf{k}\omega}$ and $\delta(K) = (1/T) \delta_{\omega,0} \delta(\mathbf{k}) = (N/T) \delta_{\omega,0} \delta_{\mathbf{k},0}$, respectively. We also use the shorthand notation $\mathbf{k}_1 + \mathbf{K}_2 = (\mathbf{k}_1 + \mathbf{k}_2, \omega_2)$. Greek superscripts denote Cartesian spin components $\alpha, \tilde{\alpha} \in \{x, y, z\}$, where $\tilde{\alpha}$ denotes dynamic η_K^{α} external legs, whereas α refers to static $m_{\mathbf{k}}^{\alpha}$ legs. Note also that spin-rotation invariance demands that only four-point vertices with pairwise identical spin component labels are finite, that is

$$\begin{aligned}
 \Gamma_{\Lambda}^{\alpha_1 \alpha_2 \alpha_3 \alpha_4}(\mathbf{k}_1, \mathbf{k}_2, \mathbf{k}_3, \mathbf{k}_4) & = \delta^{\alpha_1 \alpha_2} \delta^{\alpha_3 \alpha_4} \Gamma_{\Lambda}^{xyxy}(\mathbf{k}_1, \mathbf{k}_2, \mathbf{k}_3, \mathbf{k}_4) + \delta^{\alpha_1 \alpha_3} \delta^{\alpha_2 \alpha_4} \Gamma_{\Lambda}^{xyxy}(\mathbf{k}_1, \mathbf{k}_3, \mathbf{k}_2, \mathbf{k}_4) \\
 & + \delta^{\alpha_1 \alpha_4} \delta^{\alpha_2 \alpha_3} \Gamma_{\Lambda}^{xyxy}(\mathbf{k}_1, \mathbf{k}_4, \mathbf{k}_2, \mathbf{k}_3), \quad (6)
 \end{aligned}$$

and likewise for the mixed classical-quantum and quantum four-point vertices.

The scale-dependent static spin self-energy $\Sigma_{\Lambda}(\mathbf{k})$ determines the scale-dependent static spin susceptibility via

$$G_{\Lambda}(\mathbf{k}) = \frac{1}{J_{\Lambda}(\mathbf{k}) + \Sigma_{\Lambda}(\mathbf{k})}. \quad (7)$$

At the initial scale $\Lambda = 0$ corresponding to isolated spins, the spin self-energy is

$$\Sigma_0 = \frac{3T}{S(S+1)}, \quad (8)$$

which can be identified with the inverse susceptibility of a free spin. The dynamic spin susceptibility $G_{\Lambda}(\mathbf{k}, \omega \neq 0)$ [69] is on the other hand parametrized via the irreducible dynamic spin susceptibility $\Pi_{\Lambda}(K)$ [26] as

$$G_{\Lambda}(K) = \frac{\Pi_{\Lambda}(K)}{1 + G_{\Lambda}^{-1}(\mathbf{k}) \Pi_{\Lambda}(K)}. \quad (9)$$

For the isolated spins at $\Lambda = 0$, spin conservation implies the initial condition $\Pi_0(\omega \neq 0) = 0$. The spin FRG flow equations for the spin self-energy and polarization defined via Eqs. (7) and (9), respectively, are explicitly given by [26]

$$\partial_{\Lambda} \Sigma_{\Lambda}(\mathbf{k}) = -T \int_{\mathbf{q}} [\partial_{\Lambda} J_{\Lambda}(\mathbf{q})] G_{\Lambda}^2(\mathbf{q}) \left[\frac{1}{2} \sum_{\alpha} \Gamma_{\Lambda}^{zz\alpha\alpha}(-\mathbf{k}, \mathbf{k}, \mathbf{q}, -\mathbf{q}) + \gamma_{\Lambda}(\mathbf{k}, \mathbf{q}) \right] \quad (10)$$

and

$$-\partial_{\Lambda} \Pi_{\Lambda}(K) + \Pi_{\Lambda}^2(K) \partial_{\Lambda} \Sigma_{\Lambda}(\mathbf{k}) = -T \int_{\mathbf{q}} [\partial_{\Lambda} J_{\Lambda}(\mathbf{q})] G_{\Lambda}^2(\mathbf{q}) \tilde{\gamma}_{\Lambda}(K, \mathbf{q}), \quad (11)$$

where the contributions of the dynamic vertices are

$$\gamma_{\Lambda}(\mathbf{k}, \mathbf{q}) = \sum_{\nu \neq 0} F_{\Lambda}^2(Q) \left\{ \frac{1}{2} \sum_{\alpha} \Gamma_{\Lambda}^{zz\tilde{\alpha}\tilde{\alpha}}(-\mathbf{k}, \mathbf{k}, Q, -Q) - 2F_{\Lambda}(Q + \mathbf{k}) [\Gamma_{\Lambda}^{xy\tilde{y}\tilde{z}}(\mathbf{k}, -Q - \mathbf{k}, Q)]^2 \right\} \quad (12)$$

and

$$\begin{aligned}
 \tilde{\gamma}_{\Lambda}(K, \mathbf{q}) & = \frac{1}{2} \sum_{\alpha} \left\{ \Gamma_{\Lambda}^{\alpha\alpha\tilde{z}\tilde{z}}(-\mathbf{q}, \mathbf{q}, K, -K) + \sum_{\nu \neq 0} F_{\Lambda}^2(Q) \Gamma_{\Lambda}^{\tilde{\alpha}\tilde{\alpha}\tilde{z}\tilde{z}}(-Q, Q, K, -K) \right\} - 2F_{\Lambda}(q + K) [\Gamma_{\Lambda}^{xy\tilde{y}\tilde{z}}(\mathbf{q}, -\mathbf{q} - K, K)]^2 \\
 & + 2F_{\Lambda}^2(q, \omega) G_{\Lambda}(q + \mathbf{k}) [\Gamma_{\Lambda}^{xy\tilde{y}\tilde{z}}(-\mathbf{q} - \mathbf{k}, \mathbf{q} + \omega, K)]^2 - 2 \sum_{\nu \neq 0, -\omega} F_{\Lambda}^2(Q) F_{\Lambda}(Q + K) [\Gamma_{\Lambda}^{\tilde{y}\tilde{y}\tilde{z}}(-Q - K, Q, K)]^2. \quad (13)
 \end{aligned}$$

(a)
$$\dot{\Sigma} = \frac{1}{2} \sum_{\alpha} \left[\text{Diagram 1} + \text{Diagram 2} \right] + \text{Diagram 3}$$

(b)
$$-\dot{\Pi} + \dot{\Pi} \dot{\Sigma} \dot{\Pi} = \frac{1}{2} \sum_{\alpha} \left[\text{Diagram 4} + \text{Diagram 5} \right] + \text{Diagram 6} + \text{Diagram 7} + \text{Diagram 8}$$

FIG. 1. Graphical representations of the flow equations for (a) the static spin self-energy, Eq. (10), and (b) the dynamic spin susceptibility, Eq. (11). Colored symbols represent n -point vertices, with static and dynamic external legs denoted by straight and wavy lines, respectively. The corresponding internal lines represent the static spin susceptibility $G_{\Lambda}(\mathbf{k})$ and the dynamic propagator $F_{\Lambda}(K)$. Slashed lines denote the associated single-scale propagators [11,26]. Crosses inside loops mean that every internal line is successively replaced by its single-scale counterpart. Dots above vertices stand for scale derivatives ∂_{Λ} .

Here, $Q = (\mathbf{q}, \nu)$, $\mathbf{q} + K = (\mathbf{q} + \mathbf{k}, \omega)$, $\mathbf{q} + \omega = (\mathbf{q}, \omega)$, etc., and the dynamic propagator is

$$F_{\Lambda}(K) = \frac{1}{G_{\Lambda}(\mathbf{k}) + \Pi_{\Lambda}(K)}. \quad (14)$$

Graphical representations of the flow equations (10) and (11) are displayed in Fig. 1. Note that these flow equations for the two-point vertices are not closed: they depend on three- and four-point vertices, which in turn depend on five- and six-point vertices, and so on. In order to develop a nonperturbative truncation of this infinite hierarchy that is capable to describe also the low-temperature regime, we next explore the intricate relationships between the vertices implied by the spin algebra.

B. Spin-length sum rules

For each lattice site i the spin-operators satisfy the constraint

$$S_i^2 = S(S+1). \quad (15)$$

In spin-wave theory this constraint gives rise to the so-called kinematic interactions between spin waves. In the magnetically ordered phase of three-dimensional ferromagnets the effect of these interactions has been thoroughly investigated by Dyson [70], who concluded that kinematic interactions do not contribute to the low-temperature thermodynamics. On the other hand, in reduced dimensions or for frustrated quantum magnets the role of the spin-length constraint is expected to be more important. In fact, the low-temperature properties of quantum antiferromagnets in two dimensions have been successively modeled by a nonlinear σ -model [71–75] where interactions between spin fluctuations arise solely from the spin-length constraint. This suggests that a sensible truncation of the spin FRG flow equations for the two-dimensional J_1 - J_2 quantum Heisenberg model should also incorporate this constraint. For the scale-dependent spin susceptibility, this means that

$$\int_K G_{\Lambda}(K) = \frac{S(S+1)}{3} = \frac{T}{\Sigma_0}. \quad (16)$$

Moreover, one can also use the spin-length constraint (15) to relate higher-order n -point to $(n-2)$ -point spin correlation functions, which actually entails an infinite tower of sum rules for the vertices. We show in Appendix B that these sum rules can be generated efficiently from the exact spin FRG flow equations for the vertices in the expansion (5) by the following replacements:

- (1) $\partial_{\Lambda} J_{\Lambda}(\mathbf{q}) \rightarrow 1$,
- (2) $\partial_{\Lambda} \Sigma_{\Lambda}(\mathbf{k}) \rightarrow -1$,
- (3) $\partial_{\Lambda} f_{\Lambda} \rightarrow S(S+1)/2$,
- (4) all other Λ derivatives are set to zero.

Applied to the flow equations (10) and (11) for the two-point vertices this yields the two additional sum rules

$$1 = T \int_q G_{\Lambda}^2(\mathbf{q}) \left[\frac{1}{2} \sum_{\alpha} \Gamma_{\Lambda}^{zz\alpha\alpha}(-\mathbf{k}, \mathbf{k}, \mathbf{q}, -\mathbf{q}) + \gamma_{\Lambda}(\mathbf{k}, \mathbf{q}) \right], \quad (17a)$$

$$\Pi_{\Lambda}^2(K) = T \int_q G_{\Lambda}^2(\mathbf{q}) \tilde{\gamma}_{\Lambda}(K, \mathbf{q}). \quad (17b)$$

At the initial scale $\Lambda = 0$, these two sum rules reduce to the initial values

$$\Gamma_0^{zzzz} = 3\Gamma_0^{xyxy} = \frac{\Sigma_0^2}{5T^2} (6T + \Sigma_0) \quad (18)$$

and $\Pi_0(\omega) = 0$. Note that Eq. (18) expresses the exact static four-point vertex of an isolated spin in terms of its inverse susceptibility Σ_0 given in Eq. (8) as a consequence of the finite length of the spin operator. By considering the flow of the susceptibility sum rule (16), one can also show that it is automatically satisfied as long as the two sum rules (17a) and (17b) are fulfilled exactly. However, as soon as one truncates the flow equations and applies the inevitable approximations, this no longer holds in general. This enables us to take the three sum rules as independent constraints on the vertices.

The dynamic sum rule, Eq. (17b), can be plugged back into the associated flow equation (11), which becomes

$$\partial_{\Lambda} \Pi_{\Lambda}(K) = T \int_q [\partial_{\Lambda} J_{\Lambda}(\mathbf{q}) + \partial_{\Lambda} \Sigma_{\Lambda}(\mathbf{k})] G_{\Lambda}^2(\mathbf{q}) \tilde{\gamma}_{\Lambda}(K, \mathbf{q}). \quad (19)$$

To implement also the static sum rule, Eq. (17a), we need a suitable approximation for the static four-point vertex. Here, we are guided by the insight that for nondegenerate ground states, it is sufficient to neglect the momentum dependence of the static four-point vertex [29]. On the other hand, we expect that in a frustrated system like the J_1 - J_2 model, the momentum-dependent quantum fluctuations encoded in $\gamma_{\Lambda}(\mathbf{k}, \mathbf{q})$ are crucial. The static sum rule (17a) now tells us that in the presence of such quantum fluctuations, a momentum-independent static four-point vertex U_{Λ} is no longer sufficient to satisfy the spin-length constraint (15). Instead, the static four-point vertex must be renormalized by the momentum-dependent quantum fluctuations $\gamma_{\Lambda}(\mathbf{k}, \mathbf{q})$. In order to implement this renormalization, we make the

following ansatz for the static four-point vertex,

$$\frac{1}{2} \sum_{\alpha} \Gamma_{\Lambda}^{z\alpha\alpha}(-\mathbf{k}, \mathbf{k}, \mathbf{q}, -\mathbf{q}) = U_{\Lambda} + [V_{\Lambda}(\mathbf{k}) - 1]\gamma_{\Lambda}(\mathbf{k}, \mathbf{q}), \quad (20)$$

with initial conditions $U_0 = 5\Gamma_0^{zzzz}/6$ and $V_0(\mathbf{k}) = 1$. This turns the flow equation (10) into

$$\partial_{\Lambda} \Sigma_{\Lambda}(\mathbf{k}) = -T \int_{\mathbf{q}} [\partial_{\Lambda} J_{\Lambda}(\mathbf{q})] G_{\Lambda}^2(\mathbf{q}) [U_{\Lambda} + V_{\Lambda}(\mathbf{k})\gamma_{\Lambda}(\mathbf{k}, \mathbf{q})]. \quad (21)$$

Note that the new coupling $V_{\Lambda}(\mathbf{k})$ controls the strength of the quantum fluctuations. It is fixed by demanding that the static sum rule (17a) holds, yielding

$$V_{\Lambda}(\mathbf{k}) = \frac{1 - T U_{\Lambda} \int_{\mathbf{q}} G_{\Lambda}^2(\mathbf{q})}{T \int_{\mathbf{q}} G_{\Lambda}^2(\mathbf{q}) \gamma_{\Lambda}(\mathbf{k}, \mathbf{q})}. \quad (22)$$

The scale dependence of the remaining coupling U_{Λ} is finally set by demanding that the susceptibility sum rule (16) is conserved during the flow,

$$\partial_{\Lambda} \int_K G_{\Lambda}(K) = 0. \quad (23)$$

Inserting the flow equations (19) and (21) for the two-point vertices and solving for U_{Λ} then yields [76]

$$U_{\Lambda} = - \frac{\int_K G_{\Lambda}^2(K) [\partial_{\Lambda} J_{\Lambda}(\mathbf{k}) + \dot{\Sigma}_{\Lambda}^{(1)}(\mathbf{k})] - \int_{K(\omega \neq 0)} G_{\Lambda}^2(\mathbf{k}) F_{\Lambda}^2(K) \dot{\Pi}_{\Lambda}^{(1)}(K)}{\int_K G_{\Lambda}^2(K) \dot{\Sigma}_{\Lambda}^{(0)}(\mathbf{k}) - \int_{K(\omega \neq 0)} G_{\Lambda}^2(\mathbf{k}) F_{\Lambda}^2(K) \dot{\Pi}_{\Lambda}^{(0)}(K)}, \quad (24)$$

where we have parametrized the flow of the static self-energy as follows:

$$\partial_{\Lambda} \Sigma_{\Lambda}(\mathbf{k}) = U_{\Lambda} \dot{\Sigma}_{\Lambda}^{(0)}(\mathbf{k}) + \dot{\Sigma}_{\Lambda}^{(1)}(\mathbf{k}), \quad (25a)$$

$$\dot{\Sigma}_{\Lambda}^{(0)}(\mathbf{k}) = -T \int_{\mathbf{q}} [\partial_{\Lambda} J_{\Lambda}(\mathbf{q}) + \dot{\Sigma}_{\Lambda}^{(1)}(\mathbf{k})] G_{\Lambda}^2(\mathbf{q}), \quad (25b)$$

$$\dot{\Sigma}_{\Lambda}^{(1)}(\mathbf{k}) = - \frac{\int_{\mathbf{q}} [\partial_{\Lambda} J_{\Lambda}(\mathbf{q})] G_{\Lambda}^2(\mathbf{q}) \gamma_{\Lambda}(\mathbf{k}, \mathbf{q})}{\int_{\mathbf{q}} G_{\Lambda}^2(\mathbf{q}) \gamma_{\Lambda}(\mathbf{k}, \mathbf{q})}, \quad (25c)$$

and similarly for the flow of the dynamic two-point function,

$$\partial_{\Lambda} \Pi_{\Lambda}(K) = U_{\Lambda} \dot{\Pi}_{\Lambda}^{(0)}(K) + \dot{\Pi}_{\Lambda}^{(1)}(K), \quad (26a)$$

$$\dot{\Pi}_{\Lambda}^{(0)}(K) = T \int_{\mathbf{q}} \dot{\Sigma}_{\Lambda}^{(0)}(\mathbf{k}) \int_{\mathbf{q}'} G_{\Lambda}^2(\mathbf{q}') \tilde{\gamma}_{\Lambda}(K, \mathbf{q}), \quad (26b)$$

$$\dot{\Pi}_{\Lambda}^{(1)}(K) = T \int_{\mathbf{q}} [\partial_{\Lambda} J_{\Lambda}(\mathbf{q}) + \dot{\Sigma}_{\Lambda}^{(1)}(\mathbf{k})] G_{\Lambda}^2(\mathbf{q}) \tilde{\gamma}_{\Lambda}(K, \mathbf{q}). \quad (26c)$$

It is apparent from these expressions that satisfying the spin-length constraint (15) entails a highly nonlinear feedback mechanism between the quantum dynamics and the classical statics, which goes beyond the loop resummations of the flow equations on their own.

C. Dynamic vertices and spin conservation

Besides the spin-length constraint, the spin algebra also generates highly nontrivial quantum dynamics. This is already apparent in the complicated frequency dependence of the correlation functions and vertices of isolated spins [24,26]. In a truncation of the flow equations, these also need to be taken into account nonperturbatively if one wants to retain conservation laws of the Heisenberg model (1) throughout

the flow, such as the spin conservation $G_{\Lambda}(\mathbf{k} = 0, \omega \neq 0) = 0$ [26], which implies $\Pi_{\Lambda}(\mathbf{k} = 0, \omega \neq 0) = 0$; see Eq. (9). To develop such a truncation of the dynamic vertices, we employ the exact equations of motion of the spin correlation functions [24,26]. The equations of motion for the relevant connected three- and four-point spin correlation functions are explicitly given by

$$\begin{aligned} \omega G_{\Lambda}^{xyz}(-Q - K, Q, K) &= G_{\Lambda}(Q + K) - G_{\Lambda}(Q) + [J_{\Lambda}(\mathbf{q} + \mathbf{k}) - J_{\Lambda}(\mathbf{q})] \\ &\times G_{\Lambda}(Q + K) G_{\Lambda}(Q) + \int_{Q'} [J_{\Lambda}(\mathbf{q}' + \mathbf{k}) - J_{\Lambda}(\mathbf{q}')] \\ &\times G_{\Lambda}^{xyy}(-Q - K, Q' + K, Q, -Q'), \end{aligned} \quad (27a)$$

$$\begin{aligned} \omega G_{\Lambda}^{xyyz}(Q, -Q, -K, K) &= -G_{\Lambda}^{xyz}(Q + K, -Q, -K) \{1 + [J_{\Lambda}(\mathbf{q} + \mathbf{k}) - J_{\Lambda}(\mathbf{q})] \\ &\times G_{\Lambda}(Q)\} + (Q \leftrightarrow -Q) + \int_{Q'} [J_{\Lambda}(\mathbf{q}' + \mathbf{k}) - J_{\Lambda}(\mathbf{q}')] \\ &\times G_{\Lambda}^{xyyz}(-K, -Q, Q, Q' + K, -Q'). \end{aligned} \quad (27b)$$

Exact equations for the dynamic three- and four-point vertices can now be obtained from the tree expansion [11]. Note in particular that for $\mathbf{k} = 0$ all terms involving the exchange interaction vanish, including the loop integrations that couple to higher-order correlation functions. Only the dynamic terms generated by the spin algebra remain in this case. In order to develop a minimal truncation consistent with the spin algebra and especially the spin conservation at $\mathbf{k} = 0$, we therefore conclude that the loop integrals may be dropped. Then the dynamic three- and four-point spin correlation functions and hence also the associated vertices are entirely determined by the two-point vertices $\Sigma_{\Lambda}(\mathbf{k})$ and $\Pi_{\Lambda}(K)$. However, by neglecting the loop integrations we incur errors at order J_{Λ}^3 for

$\mathbf{k} \neq 0$. As both $\Sigma_\Lambda(\mathbf{k}) - \Sigma_0$ and $\Pi_\Lambda(K)$ are at least of order J_Λ^2 , we should then for consistency only retain terms up to linear order in these quantities, which becomes exact for $\mathbf{k} = 0$. This strategy yields the following minimal approximations for the nonvanishing dynamic three- and four-point vertices:

$$\Gamma_\Lambda^{xy\bar{z}}(\mathbf{q}, -\mathbf{q} - K, K) \approx \frac{1}{\omega}, \quad (28a)$$

$$\Gamma_\Lambda^{\bar{x}y\bar{z}}(-Q - K, Q, K) \approx \frac{1}{\omega} [\Pi_\Lambda(Q + K) - \Pi_\Lambda(Q)], \quad (28b)$$

$$\Gamma_\Lambda^{xy\bar{y}}(-\mathbf{q}, \mathbf{q}, K, -K) \approx \frac{1}{\omega^2} [\Sigma_\Lambda(\mathbf{q} + \mathbf{k}) - \Sigma_\Lambda(\mathbf{q})] + (\mathbf{q} \leftrightarrow -\mathbf{q}), \quad (28c)$$

$$\Gamma_\Lambda^{\bar{x}y\bar{y}}(-Q, Q, K, -K) \approx \frac{1}{\omega^2} \{\delta_{\omega+v,0} \Pi_\Lambda(\mathbf{q}, \omega) + (1 - \delta_{\omega+v,0}) \times [\Pi_\Lambda(Q + K) - \Pi_\Lambda(Q)]\} + (Q \leftrightarrow -Q). \quad (28d)$$

A major advantage of these expressions is that they are exact in the limit $\mathbf{k} \rightarrow 0$ and therefore satisfy spin conservation exactly. On the other hand, for $\mathbf{k} \neq 0$ Eqs. (28) are only correct to order J_Λ^2 . The contributions (12) and (13) of the dynamic vertices to the flow equations for the two-point vertices then reduce to [77]

$$\gamma_\Lambda(\mathbf{k}, \mathbf{q}) = 2 \sum_{v \neq 0} \frac{F_\Lambda^2(\mathbf{q}, v)}{v^2} [\Sigma_\Lambda(\mathbf{k} + \mathbf{q}) - \Sigma_\Lambda(\mathbf{k}) - F_\Lambda(\mathbf{q} + \mathbf{k}, v)], \quad (29a)$$

$$\tilde{\gamma}_\Lambda(K, \mathbf{q}) = \frac{2}{\omega^2} \left\{ \Sigma_\Lambda(\mathbf{q} + \mathbf{k}) - \Sigma_\Lambda(\mathbf{q}) + \sum_v F_\Lambda^2(Q) F_\Lambda(Q + K) \times [G_\Lambda(\mathbf{q} + \mathbf{k}) + \Pi_\Lambda(Q)] \times [\Pi_\Lambda(Q + K) - \Pi_\Lambda(Q)] \right\}. \quad (29b)$$

Spin conservation is ensured by construction because $\tilde{\gamma}_\Lambda(K, \mathbf{q})$ vanishes for $\mathbf{k} = 0$. Note also that the property $\tilde{\gamma}_\Lambda(K, \mathbf{q}) \propto 1/\omega^2$ implies that the ergodicity condition $\Pi_\Lambda^{-1}(\mathbf{k}, \omega \rightarrow 0) \rightarrow 0$ [26] is also automatically fulfilled.

This completes our nonperturbative truncation of the FRG flow equations. The remaining system of flow equations, Eqs. (24)–(26) together with Eqs. (29), is closed on the level of the two-point vertices $\Sigma_\Lambda(\mathbf{k})$ and $\Pi_\Lambda(K)$, while satisfying both spin-length sum rules and spin conservation. However, as we are here mainly interested in the static spin susceptibility and not in the dynamics on their own, we additionally apply a high-frequency expansion to the dynamic polarization,

$$\Pi_\Lambda(\mathbf{k}, \omega) \approx \frac{A_\Lambda(\mathbf{k})}{\omega^2} \left[1 + \mathcal{O}\left(\frac{1}{\omega^2}\right) \right]. \quad (30)$$

Anticipating that this approximation will capture the main contribution to the dynamics over a wide temperature range [29], we can then perform all Matsubara sums analytically. The resultant high-frequency approximation of the system of flow equations (24)–(26) is listed explicitly in Appendix C. It

turns out that for the J_1 - J_2 model with frustration roughly in the range $0.3 \lesssim J_2/J_1 \lesssim 0.9$, the high-frequency approximation (30) leads to unphysical results at very low temperatures: for small \mathbf{k} the function $A_\Lambda(\mathbf{k})$ can become negative, leading to instabilities. Since the dynamic polarization $\Pi_\Lambda(\mathbf{k}, \omega)$ has to be positive definite [78], this signals the breakdown of our approximation scheme. We therefore stop the flow whenever $A_\Lambda(\mathbf{k}) < 0$ for some \mathbf{k} . For the frustrated model with spin $S = 1/2$ for example, this means that depending on the strength of the frustration, we cannot reach temperatures lower than some temperature T_{\min} which is typically in the range between $J_1/13$ and $J_1/8$. However, we show in the next section that this is sufficient to obtain the full phase diagram of the J_1 - J_2 model. We have further checked that the high-frequency approximation (30) is reliable by numerically solving the flow equations without it with up to 50 positive Matsubara frequencies for several representative values of J_2/J_1 , finding no appreciable changes to the results for the static self-energy.

III. PHASE DIAGRAM

The solution of the spin FRG flow equations (24)–(26) directly generates the temperature dependence of physical spin correlation functions, in particular also of the static spin susceptibility $G(\mathbf{k}) \equiv G_{\Lambda=1}(\mathbf{k})$. Phase transitions from the paramagnetic high-temperature state to a magnetic state with ordering vector \mathbf{Q} can then be identified by the divergence of $G(\mathbf{Q})$ or equivalently the vanishing of the gap $G^{-1}(\mathbf{Q})$ at the transition temperature. We show the temperature dependence of the inverse spin susceptibility at the two classical ordering vectors in Fig. 2 for spin $S = 1/2$ and frustration values $0 \leq J_2/J_1 \leq 1$. In accordance with the Mermin-Wagner theorem [79], we observe no phase transition at finite temperatures. In order to identify possible quantum phase transitions at zero temperature, we have to keep in mind that the spin FRG flow approaches the limit $T \rightarrow 0$ only asymptotically. Therefore we have to analyze the behavior of the gap at the lowest available temperatures. A convenient way to do this is to plot $G^{-1}(\mathbf{Q})/T$ as function of J_1/T ; see Figs. 2(b) and 2(d). For a gapped state with finite $G^{-1}(\mathbf{Q})$ at $T = 0$, this curve grows linearly at large J_1/T . If the ground state on the other hand possesses long-range order, $G^{-1}(\mathbf{Q})/T$ approaches a constant. In this manner, we find that at small next-nearest neighbor coupling $J_2 < 0.449J_1$, the gap of the Néel state vanishes for $T \rightarrow 0$, suggesting the expected Néel ordered ground state. In the opposite limit of large next-nearest neighbor coupling, $J_2 > 0.654J_1$, we likewise find the expected stripe ordered ground state. In the intermediate regime $0.449 \leq J_2/J_1 \leq 0.654$ of strong frustration the system remains gapped. We therefore identify the ground state in this regime as a quantum paramagnet without magnetic long-range order, in good quantitative agreement with the literature [41,45,50,52–54,56–58,62–64]. The residual gaps of the Néel and stripe states at the end of the spin FRG flow are displayed in Fig. 3, where one clearly sees the emergence of a gapped quantum paramagnet at strong frustration. Note also that the point where the states with Néel and stripe ordering are degenerate is shifted upwards from the classical value $J_2/J_1 = 0.5$ to $J_2/J_1 \approx 0.54$ by the strong quantum fluctuations.

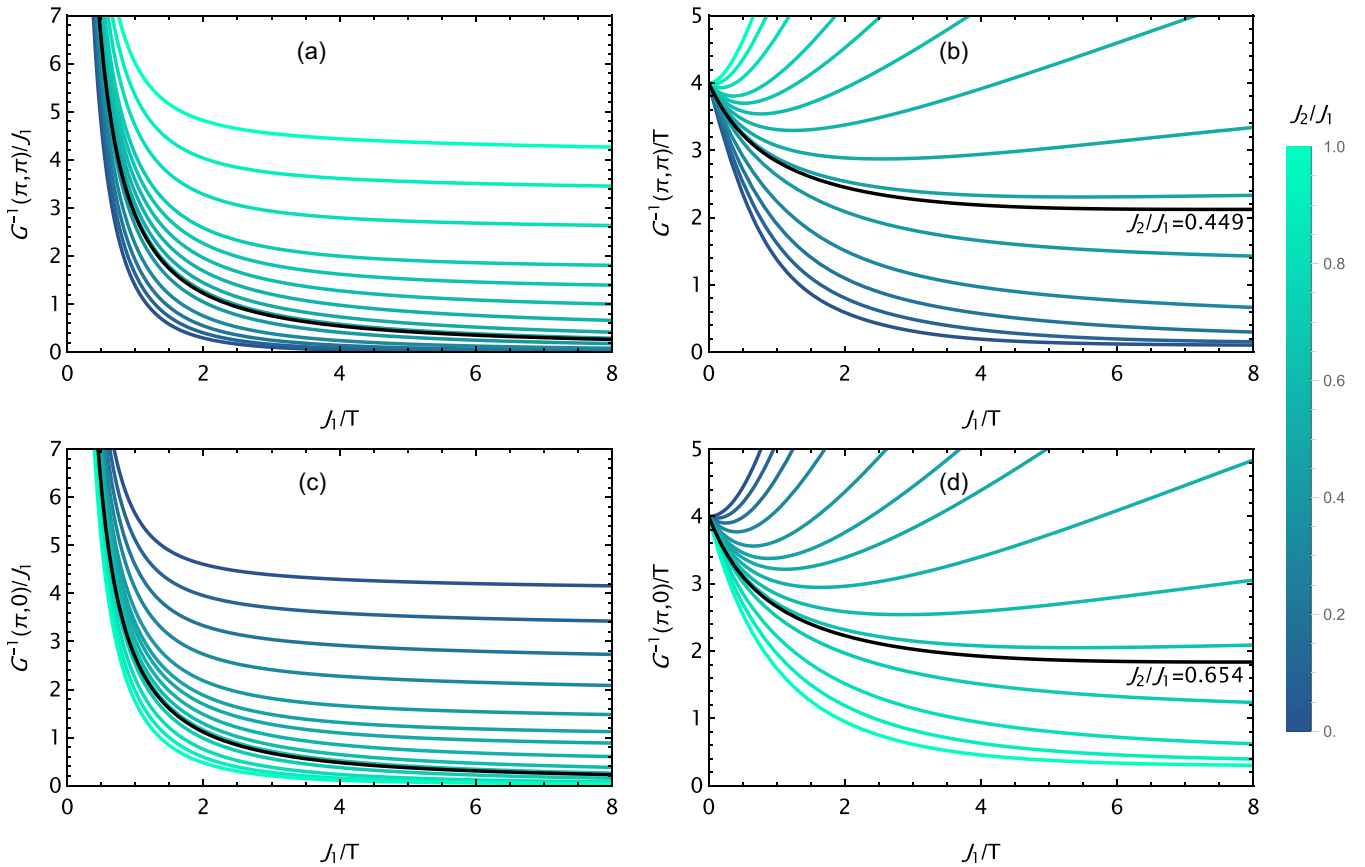


FIG. 2. Temperature dependence of the inverse spin susceptibility for spin $S = 1/2$ at the Néel [(a) and (b)] and stripe [(c) and (d)] ordering vectors, $\mathbf{Q} = (\pi, \pi)$ and $\mathbf{Q} = (\pi, 0)$ respectively, for frustration values $0 \leq J_2/J_1 \leq 1$. (a) and (c) display the absolute value of $G^{-1}(\mathbf{Q})$, whereas (b) and (d) show the value relative to the temperature T . The latter depiction facilitates the distinction between gapless states, where $G^{-1}(\mathbf{Q})/T$ approaches a constant for large J_1/T , and gapped states, where it increases linearly. The phase boundaries of Fig. 3 are determined as the values of J_2/J_1 for which $G^{-1}(\mathbf{Q})/T$ is asymptotically flat at low temperatures. These special curves are plotted as black solid lines. We show the temperature dependence only up to $J_1/T = 8$ because at lower temperatures the dynamic coefficient $A_\lambda(\mathbf{k})$ flows to unphysical negative values for highly frustrated values of J_2/J_1 .

While our spin FRG flow predicts the existence of the intermediate paramagnetic phase, it unfortunately does not

make any statements about its nature. Thus we cannot at this stage distinguish between the possible spin liquid and valence bond states discussed in the literature [37,40,42,44,46,49,51–55,57,58,62,64]. We also cannot exclude the possibility of a gapless spin liquid state [54,62,63] at small J_2 , since it is hard to distinguish from the Néel state in our approach. This is however not an intrinsic limitation of the spin FRG, but rather of our truncation, which focuses on the two-point spin correlation function. A more sophisticated truncation capable of investigating dimer correlation functions would have to include the momentum and frequency dependence of the dynamic four-point vertex in an unbiased manner, which is beyond the scope of this work. An alternative approach would be to add small perturbations to the exchange interaction that favor certain types of order. This was done in Ref. [14] for the pseudofermion flow. As these perturbations necessarily break translational invariance, we do not pursue this approach here. We should also mention that we cannot draw any reliable conclusions about the order of the phase transitions from the gap values in Fig. 3. The reason for this is that we stop the flow at a finite (small) temperature, which washes out the sharp step expected for a first order transition.

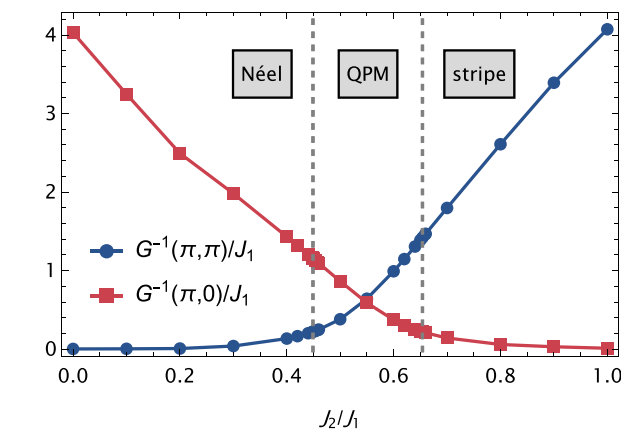


FIG. 3. Residual gaps of the Néel and stripe states, $\mathbf{Q} = (\pi, \pi)$ and $\mathbf{Q} = (\pi, 0)$ respectively, at the end of the spin FRG flow, for spin $S = 1/2$. In the regime of strong frustration for $0.449 \leq J_2/J_1 \leq 0.654$, marked by the dashed gray lines, we identify a gapped quantum paramagnet (QPM). Solid lines are guides to the eye.

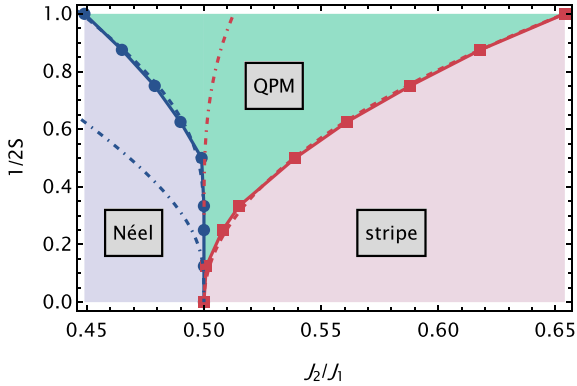


FIG. 4. Ground state phase diagram of the J_1 - J_2 model as function of frustration J_2/J_1 and spin quantum number $1/2S$, exhibiting Néel, stripe and intermediate quantum paramagnet (QPM) phases. Solid lines are guides to the eye. The dashed lines are the fits (31) for the phase boundaries. Dash-dotted lines of the corresponding colors represent the linear spin-wave theory prediction of Ref. [30] for the phase boundaries, which significantly underestimates the extent of the paramagnetic phase for small S .

A major advantage of the spin FRG approach to quantum spin systems is that the spin quantum number S only enters as a parameter into the vertex functions. We can therefore investigate arbitrary values (including noninteger and non-half-integer values) of S without any additional numerical or analytical effort. This allows us to tune not only the frustration but also the importance of quantum fluctuations, which vanish for $S \rightarrow \infty$. The resulting phase diagram as function of frustration J_2/J_1 and spin quantum number $1/2S$ is shown in Fig. 4. Similar to spin-wave theory [30], our spin FRG predicts the existence of the quantum paramagnetic phase for spin $S \lesssim 5$. For even larger spin, only the two classically ordered phases remain, with a phase transition at the point of classical degeneracy $J_2/J_1 = 0.5$. Qualitatively, the behavior of the phase boundaries is also as predicted by linear spin wave theory [30]; the spin FRG phase boundaries are well approximated by

$$\frac{1}{2S} = \frac{-2.95}{\ln(1/2 - J_2/J_1)} \quad (\text{Néel}), \quad (31a)$$

$$\frac{1}{2S} = 2.55\sqrt{J_2/J_1 - 1/2} \quad (\text{stripe}). \quad (31b)$$

These curves are shown as dashed blue and red lines in Fig. 4, respectively. However, the quantitative picture is rather different from the predictions of spin-wave theory [30] that are for comparison plotted as dash-dotted lines in Fig. 4, with a significantly larger and rather asymmetric paramagnetic region that is wider for $J_2/J_1 > 0.5$ than for $J_2/J_1 < 0.5$. Thus it appears that the magnitude of frustration-induced quantum fluctuations are overestimated by spin-wave theory for the Néel state and severely underestimated for the stripe state.

IV. SUMMARY AND OUTLOOK

In this work, we have studied the zero-temperature phase diagram of the paradigmatic J_1 - J_2 quantum Heisenberg model on a square lattice for arbitrary spin quantum number S using an advanced implementation [29] of the spin FRG approach

proposed in Ref. [22]. Let us summarize the main technical advances reported in this work.

(1) The innocent looking spin-length constraint $S_i^2 = S(S+1)$ implies an infinite tower of sum rules involving vertices of different order which can be elegantly derived using our spin FRG formalism.

(2) These sum rules can be used to construct nonperturbative truncations of the formally exact spin FRG flow equations.

(3) For frustrated magnets in reduced dimensions the implementation of these sum rules and the constraints imposed by spin conservation and ergodicity are crucial to construct sensible truncations of the spin FRG flow equations.

(4) In contrast to the pseudofermion FRG approach [14,15], the implementation of our spin FRG for frustrated magnets does not require heavy numerical calculations; the results presented in this work have been obtained in a few minutes on a desktop computer. It is also not necessary to perform finite-size scaling to detect phase transitions between long-range ordered and paramagnetic phases in the spin FRG, unlike in the pseudofermion and pseudo-Majorana FRG implementations. Which method is ultimately preferable for the study of frustrated quantum magnets of course also depends on their respective quantitative accuracy. In this respect, it would be desirable to compare the spin FRG with pseudofermion and pseudo-Majorana FRG in benchmark systems where exact results are known by other methods.

(5) The spin FRG allows us to investigate quantum spin systems for arbitrary real values of the spin quantum number S , without additional technical modifications or numerical costs. While implementations of the pseudofermion FRG for $S > 1/2$ exist [15,80,81], they come with additional technical complications because each spin- S operator is represented by $2S$ copies of spin-1/2 operators, which are then expressed in terms of pseudofermions with an additional flavor index. Due to this construction, they are also restricted to integer or half-integer values of S .

The main physical result obtained in this work is the zero-temperature phase diagram of the J_1 - J_2 model as a function of J_2/J_1 and the inverse spin quantum number $1/2S$ shown in Fig. 4. Although spin-wave theory produces a qualitatively similar phase diagram, the shape of the phase boundaries obtained by us is more asymmetric and the extension of the paramagnetic phase significantly larger than predicted by spin-wave theory.

Our approach offers many promising opportunities for further research. The inclusion of an external magnetic field is straightforward and does not add any significant complexity. The door is now wide open to use our spin FRG approach to study ground state properties of more complicated models for frustrated magnets involving other lattices and less symmetric exchange couplings.

ACKNOWLEDGMENTS

We thank Björn Sbierski and Benedikt Schneider for useful discussions and detailed comments on the manuscript. This work was financially supported by the Deutsche Forschungsgemeinschaft (DFG, German Research Foundation) through Project No. 431190042.

APPENDIX A: TEMPERATURE RESCALING

A significant advantage of the multiplicative deformation scheme (4) is that in the absence of external magnetic fields, the temperature dependence can be removed from the problem entirely by rescaling the deformation parameter and Matsubara frequencies as

$$\Lambda = \bar{\Lambda}T, \quad \bar{\Lambda} \in [0, 1/T], \quad (\text{A1a})$$

$$\omega = \bar{\omega}T. \quad (\text{A1b})$$

It is then straightforward to see from the generating functional (5) that the vertices should be rescaled as

$$\Gamma_{\Lambda}^{\alpha_1 \dots \alpha_n \tilde{\alpha}_1 \dots \tilde{\alpha}_m}(\mathbf{k}_1, \dots, \mathbf{k}_n, (\mathbf{q}_1, \omega_1), \dots, (\mathbf{q}_m, \omega_m)) = T^{1-m} \bar{\Gamma}_{\bar{\Lambda}=\Lambda/T}^{\alpha_1 \dots \alpha_n \tilde{\alpha}_1 \dots \tilde{\alpha}_m}(\mathbf{k}_1, \dots, \mathbf{k}_n, (\mathbf{q}_1, \omega_1/T), \dots, (\mathbf{q}_m, \omega_m/T)), \quad (\text{A2a})$$

$$\bar{\Gamma}_{\bar{\Lambda}}^{\alpha_1 \dots \alpha_n \tilde{\alpha}_1 \dots \tilde{\alpha}_m}(\mathbf{k}_1, \dots, \mathbf{k}_n, (\mathbf{q}_1, \bar{\omega}_1), \dots, (\mathbf{q}_m, \bar{\omega}_m)) = T^{m-1} \Gamma_{\Lambda=\bar{\Lambda}T}^{\alpha_1 \dots \alpha_n \tilde{\alpha}_1 \dots \tilde{\alpha}_m}(\mathbf{k}_1, \dots, \mathbf{k}_n, (\mathbf{q}_1, \bar{\omega}_1 T), \dots, (\mathbf{q}_m, \bar{\omega}_m T)), \quad (\text{A2b})$$

where the rescaled $\bar{\Gamma}_{\bar{\Lambda}}$ vertices do not depend explicitly on the temperature T . In this way, we obtain an effectively T -independent problem with $T \rightarrow 1$ at fixed $\bar{\Lambda}$. The T -dependence is then generated by flowing from $\bar{\Lambda} = 0$, corresponding to $T \rightarrow \infty$, to $\bar{\Lambda} = 1/T$. In this form, the only remaining dimensionful quantities are $\bar{\Lambda}$ and $J(\mathbf{k})$, which always appear as dimensionless product $\bar{\Lambda}J(\mathbf{k})$. This rescaling also makes it obvious that by expanding the spin FRG flow equations in powers of $\bar{\Lambda}J(\mathbf{k})$ we obtain the high-temperature expansion for the spin vertices.

APPENDIX B: SPIN-LENGTH SUM RULES FROM SPIN FRG FLOW EQUATIONS

In order to efficiently derive the sum rules associated with the spin-length constraint (15), we write a general deformed Heisenberg Hamiltonian as

$$\mathcal{H}_{\Lambda} = \frac{1}{2} \sum_{ij} J_{ij}^{\Lambda} \mathbf{S}_i \cdot \mathbf{S}_j \quad (\text{B1a})$$

$$= \frac{1}{2} \sum_{ij} [J_{ij}^{\Lambda} + \delta_{ij} C_{\Lambda} - \delta_{ij} C_{\Lambda}] \mathbf{S}_i \cdot \mathbf{S}_j \quad (\text{B1b})$$

$$= \frac{1}{2} \sum_{ij} (J_{ij}^{\Lambda} + \delta_{ij} C_{\Lambda}) \mathbf{S}_i \cdot \mathbf{S}_j - \frac{N}{2} C_{\Lambda} S(S+1), \quad (\text{B1c})$$

with arbitrary, scale-dependent C_{Λ} . This rewriting leads to the following modifications in the flow equations.

- (1) The constant energy shift adds an additional term

$$-\frac{1}{2} \partial_{\Lambda} C_{\Lambda} S(S+1) \quad (\text{B2})$$

to the right-hand side of the flow equation of the free energy density f_{Λ} .

- (2) The on-site shift in the exchange coupling results in the replacement

$$\partial_{\Lambda} J_{\Lambda}(\mathbf{q}) \rightarrow \partial_{\Lambda} J_{\Lambda}(\mathbf{q}) + \partial_{\Lambda} C_{\Lambda} \quad (\text{B3})$$

everywhere in all flow equations.

- (3) The scale-dependent static spin susceptibility is now parametrized as

$$G_{\Lambda}(\mathbf{k}) = \frac{1}{J_{\Lambda}(\mathbf{k}) + C_{\Lambda} + \tilde{\Sigma}_{\Lambda}(\mathbf{k})}. \quad (\text{B4})$$

The crucial point is now that we did not modify the system at all, but only added a zero to the Hamiltonian regardless of the value of Λ . Hence, all correlation functions must remain independent of C_{Λ} . Comparing with the original parametrization (7) of the static spin susceptibility, we immediately infer

$$\tilde{\Sigma}_{\Lambda}(\mathbf{k}) = \Sigma_{\Lambda}(\mathbf{k}) - C_{\Lambda}, \quad (\text{B5})$$

where $\Sigma_{\Lambda}(\mathbf{k})$ is independent of C_{Λ} . As all other vertex functions in the hybrid functional are defined in terms of spin correlation functions [26], it follows that they must be independent of C_{Λ} . Consequently, all $\partial_{\Lambda} C_{\Lambda}$ -contributions to their flow equations must cancel. For example, the flow of the free energy density is given by

$$\partial_{\Lambda} f_{\Lambda} = \frac{3}{2} \int_K [\partial_{\Lambda} J_{\Lambda}(\mathbf{k})] G_{\Lambda}(K) \quad \text{at } C_{\Lambda} = 0 \quad (\text{B6a})$$

$$= \frac{3}{2} \int_K [\partial_{\Lambda} J_{\Lambda}(\mathbf{k}) + \partial_{\Lambda} C_{\Lambda}] G_{\Lambda}(K) - \frac{1}{2} \partial_{\Lambda} C_{\Lambda} S(S+1) \quad (\text{B6b})$$

$$= \frac{3}{2} \int_K [\partial_{\Lambda} J_{\Lambda}(\mathbf{k})] G_{\Lambda}(K) + \frac{3}{2} [\partial_{\Lambda} C_{\Lambda}] \left[\int_K G_{\Lambda}(K) - \frac{S(S+1)}{3} \right]. \quad (\text{B6c})$$

Comparing the first and last line of the above yields the susceptibility sum rule (16). This scheme can be applied in the same way to each spin FRG flow equation to yield an associated sum rule for the vertices. In practice, this means that one can apply the rules (1)–(4) given in Sec. II B to any spin FRG flow equation to elegantly derive the associated sum rule, since these rules generate precisely the $\partial_{\Lambda} C_{\Lambda}$ contributions that have to vanish in order to guarantee consistency of the correlation functions. Note also that because the hierarchy of spin FRG flow equations is infinite, there is likewise an infinite tower of spin-length sum rules.

APPENDIX C: DYNAMICS IN THE HIGH-FREQUENCY APPROXIMATION

In this Appendix, we give explicit expressions for the flow equations (24)–(26) in the high-frequency approximation (30). They depend on the following four distinct

Matsubara sums:

$$S_1(x) = \sum_{\nu \neq 0} \frac{(\nu/T)^2}{[(\nu/T)^2 + x]^2} = \frac{\sqrt{x} - \sinh(\sqrt{x})}{4\sqrt{x}[1 - \cosh(\sqrt{x})]}, \quad (\text{C1a})$$

$$\begin{aligned} S_2(x, y) &= \sum_{\nu \neq 0} \frac{(\nu/T)^4}{[(\nu/T)^2 + x]^2[(\nu/T)^2 + y]} \\ &= \frac{1}{8(x-y)^2} [2\sqrt{x}(x-3y) \coth(\sqrt{x}/2) - x(x-y) \operatorname{csch}^2(\sqrt{x}/2) + 4y^{3/2} \coth(\sqrt{y}/2)], \end{aligned} \quad (\text{C1b})$$

$$\begin{aligned} S_3(x, y, z) &= \lim_{\omega \rightarrow \infty} \left[\omega^2 \sum_{\nu} \frac{(\nu/T)^4}{[(\nu/T)^2 + x]^2} \frac{(\nu/T + \omega/T)^2}{(\nu/T + \omega/T)^2 + y} \left(1 + \frac{zx}{(\nu/T)^2} \right) \left(\frac{y}{(\nu/T + \omega/T)^2} - \frac{zx}{(\nu/T)^2} \right) \right] \\ &= \frac{1}{8} [4\sqrt{y} \coth(\sqrt{y}/2) - z\sqrt{x} \operatorname{csch}^2(\sqrt{x}/2) [(z-1)\sqrt{x} + (z+1) \sinh(\sqrt{x})]], \end{aligned} \quad (\text{C1c})$$

$$S_4(x) = \sum_{\nu} \frac{x^2}{[(\nu/T)^2 + x]^2} = \frac{x + \sqrt{x} \sinh(\sqrt{x})}{4[\cosh(\sqrt{x}) - 1]}. \quad (\text{C1d})$$

Writing the leading coefficient $A_{\Lambda}(\mathbf{k})$ in the high-frequency expansion (30) of the polarization $\Pi_{\Lambda}(\mathbf{k}, \omega)$ in the form

$$A_{\Lambda}(\mathbf{k}) = T^2 G_{\Lambda}(\mathbf{k}) \Omega_{\Lambda}(\mathbf{k}), \quad (\text{C2})$$

we find that the dynamic diagrams (29a) that contribute to the static self-energy are given by

$$T^2 G_{\Lambda}^2(\mathbf{q}) \gamma_{\Lambda}(\mathbf{k}, \mathbf{q}) = 2[\Sigma_{\Lambda}(\mathbf{k} + \mathbf{q}) - \Sigma_{\Lambda}(\mathbf{k})] S_1(\Omega_{\Lambda}(\mathbf{q})) - 2G_{\Lambda}^{-1}(\mathbf{q} + \mathbf{k}) S_2(\Omega_{\Lambda}(\mathbf{q}), \Omega_{\Lambda}(\mathbf{q} + \mathbf{k})). \quad (\text{C3})$$

The polarization coefficient $A_{\Lambda}(\mathbf{k})$ itself satisfies the flow equation

$$\partial_{\Lambda} A_{\Lambda}(\mathbf{k}) = U_{\Lambda} \dot{A}_{\Lambda}^{(0)}(\mathbf{k}) + \dot{A}_{\Lambda}^{(1)}(\mathbf{k}), \quad (\text{C4a})$$

$$\dot{A}_{\Lambda}^{(0)}(\mathbf{k}) = T \dot{\Sigma}_{\Lambda}^{(0)}(\mathbf{k}) \int_{\mathbf{q}} \tilde{\gamma}_{\Lambda}^{(A)}(\mathbf{k}, \mathbf{q}), \quad (\text{C4b})$$

$$\dot{A}_{\Lambda}^{(1)}(\mathbf{k}) = T \int_{\mathbf{q}} [\partial_{\Lambda} J_{\Lambda}(\mathbf{q}) + \dot{\Sigma}_{\Lambda}^{(1)}(\mathbf{k})] \tilde{\gamma}_{\Lambda}^{(A)}(\mathbf{k}, \mathbf{q}), \quad (\text{C4c})$$

$$\tilde{\gamma}_{\Lambda}^{(A)}(\mathbf{k}, \mathbf{q}) = 2G_{\Lambda}^2(\mathbf{q}) [\Sigma_{\Lambda}(\mathbf{q} + \mathbf{k}) - \Sigma_{\Lambda}(\mathbf{q})] + 2G_{\Lambda}(\mathbf{q} + \mathbf{k}) S_3(\Omega_{\Lambda}(\mathbf{q}), \Omega_{\Lambda}(\mathbf{q} + \mathbf{k}), G_{\Lambda}^{-1}(\mathbf{q} + \mathbf{k}) G_{\Lambda}(\mathbf{q})). \quad (\text{C4d})$$

Finally, the static four-point vertex in Eq. (24) reduces to

$$U_{\Lambda} = - \frac{T^2 \int_{\mathbf{k}} G_{\Lambda}^2(\mathbf{k}) S_4(\Omega_{\Lambda}(\mathbf{k})) [\partial_{\Lambda} J_{\Lambda}(\mathbf{k}) + \dot{\Sigma}_{\Lambda}^{(1)}(\mathbf{k})] - \int_{\mathbf{k}} S_1(\Omega_{\Lambda}(\mathbf{k})) \dot{A}_{\Lambda}^{(1)}(\mathbf{k})}{T^2 \int_{\mathbf{k}} G_{\Lambda}^2(\mathbf{k}) S_4(\Omega_{\Lambda}(\mathbf{k})) \dot{\Sigma}_{\Lambda}^{(0)}(\mathbf{k}) - \int_{\mathbf{k}} S_1(\Omega_{\Lambda}(\mathbf{k})) \dot{A}_{\Lambda}^{(0)}(\mathbf{k})}. \quad (\text{C5})$$

-
- [1] L. Balents, Spin liquids in frustrated magnets, *Nature (London)* **464**, 199 (2010).
- [2] A. W. Sandvik, Computational studies of quantum spin systems, *AIP Conf. Proc.* **1297**, 135 (2010).
- [3] L. Savary and L. Balents, Quantum spin liquids: a review, *Rep. Prog. Phys.* **80**, 016502 (2017).
- [4] Y. Zhou, K. Kanoda, and T.-K. Ng, Quantum spin liquid states, *Rev. Mod. Phys.* **89**, 025003 (2017).
- [5] H. T. Diep, *Frustrated Spin Systems*, 3rd ed. (World Scientific, Singapore, 2020).
- [6] S. R. White, Density matrix formulation for quantum renormalization groups, *Phys. Rev. Lett.* **69**, 2863 (1992).
- [7] U. Schollwöck, The density-matrix renormalization group, *Rev. Mod. Phys.* **77**, 259 (2005).
- [8] C. Wetterich, Exact evolution equation for the effective potential, *Phys. Lett. B* **301**, 90 (1993).
- [9] J. Berges, N. Tetradis, and C. Wetterich, Non-perturbative renormalization flow in quantum field theory and statistical physics, *Phys. Rep.* **363**, 223 (2002).
- [10] J. M. Pawłowski, Aspects of the functional renormalisation group, *Ann. Phys.* **322**, 2831 (2007).
- [11] P. Kopietz, L. Bartosch, and F. Schütz, *Introduction to the Functional Renormalization Group* (Springer, Berlin, 2010).
- [12] W. Metzner, M. Salmhofer, C. Honerkamp, V. Meden, and K. Schönhammer, Functional renormalization group approach to correlated fermion systems, *Rev. Mod. Phys.* **84**, 299 (2012).
- [13] N. Dupuis, L. Canet, A. Eichhorn, W. Metzner, J. M. Pawłowski, M. Tissier, and N. Wschebor, The nonperturbative functional renormalization group and its applications, *Phys. Rep.* **910**, 1 (2021).

- [14] J. Reuther and P. Wölfle, J_1 - J_2 frustrated two-dimensional Heisenberg model: Random phase approximation and functional renormalization group, *Phys. Rev. B* **81**, 144410 (2010).
- [15] T. Müller, D. Kiese, N. Niggemann, B. Sbierski, J. Reuther, S. Trebst, R. Thomale, and Y. Iqbal, Pseudo-fermion functional renormalization group for spin models, *Rep. Prog. Phys.* **87**, 036501 (2024).
- [16] J. L. Martin, Generalized classical dynamics, and the ‘classical analogue’ of a Fermioscillator, *Proc. R. Soc. London A* **251**, 536 (1959).
- [17] A. M. Tsvelik, New fermionic description of quantum spin liquid state, *Phys. Rev. Lett.* **69**, 2142 (1992).
- [18] N. Niggemann, B. Sbierski, and J. Reuther, Frustrated quantum spins at finite temperature: Pseudo-Majorana functional renormalization group approach, *Phys. Rev. B* **103**, 104431 (2021).
- [19] N. Niggemann, J. Reuther, and B. Sbierski, Quantitative functional renormalization for three-dimensional quantum Heisenberg models, *SciPost Phys.* **12**, 156 (2022).
- [20] V. N. Popov and S. A. Fedotov, The functional-integration method and diagram technique for spin systems, *Zh. Eksp. Teor. Fiz.* **94**, 183 (1988) [*Sov. Phys. JETP* **67**, 535 (1988)].
- [21] B. Schneider, D. Kiese, and B. Sbierski, Taming pseudofermion functional renormalization for quantum spins: Finite temperatures and the Popov-Fedotov trick, *Phys. Rev. B* **106**, 235113 (2022).
- [22] J. Krieg and P. Kopietz, Exact renormalization group for quantum spin systems, *Phys. Rev. B* **99**, 060403(R) (2019).
- [23] D. Tarasevych, J. Krieg, and P. Kopietz, A rich man’s derivation of scaling laws for the Kondo model, *Phys. Rev. B* **98**, 235133 (2018).
- [24] R. Goll, D. Tarasevych, J. Krieg, and P. Kopietz, Spin functional renormalization group for quantum Heisenberg ferromagnets: Magnetization and magnon damping in two dimensions, *Phys. Rev. B* **100**, 174424 (2019).
- [25] R. Goll, A. Rückriegel, and P. Kopietz, Zero-magnon sound in quantum Heisenberg ferromagnets, *Phys. Rev. B* **102**, 224437 (2020).
- [26] D. Tarasevych and P. Kopietz, Dissipative spin dynamics in hot quantum paramagnets, *Phys. Rev. B* **104**, 024423 (2021).
- [27] D. Tarasevych and P. Kopietz, Critical spin dynamics of Heisenberg ferromagnets revisited, *Phys. Rev. B* **105**, 024403 (2022).
- [28] A. Rückriegel, J. Arnold, R. Goll, and P. Kopietz, Spin functional renormalization group for dimerized quantum spin systems, *Phys. Rev. B* **105**, 224406 (2022).
- [29] D. Tarasevych, A. Rückriegel, S. Keupert, V. Mitsioannou, and P. Kopietz, Spin-functional renormalization group for the $J_1J_2J_3$ quantum Heisenberg model, *Phys. Rev. B* **106**, 174412 (2022).
- [30] P. Chandra and B. Douçot, Possible spin-liquid state at large S for the frustrated square Heisenberg lattice, *Phys. Rev. B* **38**, 9335(R) (1988).
- [31] I. G. Gochev, Theory of the Néel and collinear phases in the J_1 - J_2 model of a spin-1/2 square-lattice frustrated antiferromagnet, *Phys. Rev. B* **49**, 9594 (1994).
- [32] A. V. Dotsenko and O. P. Sushkov, Quantum phase transition in the frustrated Heisenberg antiferromagnet, *Phys. Rev. B* **50**, 13821 (1994).
- [33] L. Siurakshina, D. Ihle, and R. Hayn, Magnetic order and finite-temperature properties of the two-dimensional frustrated Heisenberg model, *Phys. Rev. B* **64**, 104406 (2001).
- [34] A. F. Barabanov and V. M. Beresovsky, On the theory of the two-dimensional Heisenberg antiferromagnet with frustration on a square lattice, *J. Phys. Soc. Jpn.* **63**, 3974 (1994).
- [35] A. F. Barabanov and V. M. Berezovskii, Second-order phase transitions in a frustrated two-dimensional Heisenberg antiferromagnet, *Zh. Eksp. Teor. Fiz.* **106**, 1156 (1994) [*Sov. Phys. JETP* **79**, 627 (1994)].
- [36] D. Sasamoto and T. Morinari, General formula for the green’s function approach to the spin-1/2 antiferromagnetic Heisenberg model, *J. Phys. Soc. Jpn.* **93**, 024704 (2024).
- [37] N. Read and S. Sachdev, Large- N expansion for frustrated quantum antiferromagnets, *Phys. Rev. Lett.* **66**, 1773 (1991).
- [38] T. Einarsson and H. Johannesson, Effective-action approach to the frustrated Heisenberg antiferromagnet in two dimensions, *Phys. Rev. B* **43**, 5867 (1991).
- [39] T. Einarsson, P. Fröjdh, and H. Johannesson, Weakly frustrated spin-1/2 Heisenberg antiferromagnet in two dimensions: Thermodynamic parameters and the stability of the Néel state, *Phys. Rev. B* **45**, 13121(R) (1992).
- [40] M. E. Zhitomirsky and K. Ueda, Valence-bond crystal phase of a frustrated spin-1/2 square-lattice antiferromagnet, *Phys. Rev. B* **54**, 9007 (1996).
- [41] V. N. Kotov, J. Oitmaa, O. P. Sushkov, and Z. Weihong, Low-energy singlet and triplet excitations in the spin-liquid phase of the two-dimensional $J_1 - J_2$ model, *Phys. Rev. B* **60**, 14613 (1999).
- [42] V. N. Kotov and O. P. Sushkov, Nature of the transition from the spontaneously dimerized to the Néel phase in the two-dimensional $J_1 - J_2$ model, *Phys. Rev. B* **61**, 11820 (2000).
- [43] R. L. Doretto, Plaquette valence-bond solid in the square-lattice J_1 - J_2 antiferromagnet Heisenberg model: A bond operator approach, *Phys. Rev. B* **89**, 104415 (2014).
- [44] M. P. Gelfand, R. R. P. Singh, and D. A. Huse, Zero-temperature ordering in two-dimensional frustrated quantum Heisenberg antiferromagnets, *Phys. Rev. B* **40**, 10801 (1989).
- [45] J. Oitmaa and Z. Weihong, Series expansion for the J_1 - J_2 Heisenberg antiferromagnet on a square lattice, *Phys. Rev. B* **54**, 3022 (1996).
- [46] O. P. Sushkov, J. Oitmaa, and Z. Weihong, Quantum phase transitions in the two-dimensional $J_1 - J_2$ model, *Phys. Rev. B* **63**, 104420 (2001).
- [47] J. Sirker, Z. Weihong, O. P. Sushkov, and J. Oitmaa, $J_1 - J_2$ model: First-order phase transition versus deconfinement of spinons, *Phys. Rev. B* **73**, 184420 (2006).
- [48] E. Dagotto and A. Moreo, Phase diagram of the frustrated spin-1/2 Heisenberg antiferromagnet in 2 dimensions, *Phys. Rev. Lett.* **63**, 2148 (1989).
- [49] F. Figueirido, A. Karlhede, S. Kivelson, S. Sondhi, M. Rocek, and D. S. Rokhsar, Exact diagonalization of finite frustrated spin-1/2 Heisenberg models, *Phys. Rev. B* **41**, 4619 (1990).
- [50] L. Capriotti and S. Sorella, Spontaneous plaquette dimerization in the J_1 - J_2 Heisenberg model, *Phys. Rev. Lett.* **84**, 3173 (2000).
- [51] M. S. L. du Croo de Jongh, J. M. J. van Leeuwen, and W. van Saarloos, Incorporation of density-matrix wave

- functions in Monte Carlo simulations: Application to the frustrated Heisenberg model, *Phys. Rev. B* **62**, 14844 (2000).
- [52] H.-C. Jiang, H. Yao, and L. Balents, Spin liquid ground state of the spin- $\frac{1}{2}$ square J_1 - J_2 Heisenberg model, *Phys. Rev. B* **86**, 024424 (2012).
- [53] S.-S. Gong, W. Zhu, D. N. Sheng, O. I. Motrunich, and M. P. A. Fisher, Plaquette ordered phase and quantum phase diagram in the spin- $\frac{1}{2}$ $J_1 - J_2$ square Heisenberg model, *Phys. Rev. Lett.* **113**, 027201 (2014).
- [54] L. Wang and A. W. Sandvik, Critical level crossings and gapless spin liquid in the square-lattice spin- $1/2$ $J_1 - J_2$ Heisenberg antiferromagnet, *Phys. Rev. Lett.* **121**, 107202 (2018).
- [55] X. Qian and M. Qin, Absence of spin liquid phase in the $J_1 - J_2$ Heisenberg model on the square lattice, *Phys. Rev. B* **109**, L161103 (2024).
- [56] R. Darradi, O. Derzhko, R. Zinke, J. Schulenburg, S. E. Krüger, and J. Richter, Ground state phases of the spin- $1/2$ $J_1 - J_2$ Heisenberg antiferromagnet on the square lattice: A high-order coupled cluster treatment, *Phys. Rev. B* **78**, 214415 (2008).
- [57] L. Isaev, G. Ortiz, and J. Dukelsky, Hierarchical mean-field approach to the $J_1 - J_2$ Heisenberg model on a square lattice, *Phys. Rev. B* **79**, 024409 (2009).
- [58] M. J. de Oliveira, Phase diagram of the spin- $1/2$ Heisenberg antiferromagnet on a square lattice with nearest- and next-nearest-neighbor couplings, *Phys. Rev. B* **43**, 6181 (1991).
- [59] L. Capriotti, F. Becca, A. Parola, and S. Sorella, Resonating valence bond wave functions for strongly frustrated spin systems, *Phys. Rev. Lett.* **87**, 097201 (2001).
- [60] V. Murg, F. Verstraete, and J. I. Cirac, Exploring frustrated spin systems using projected entangled pair states, *Phys. Rev. B* **79**, 195119 (2009).
- [61] X. Zhang and K. S. D. Beach, Resonating valence bond trial wave functions with both static and dynamically determined Marshall sign structure, *Phys. Rev. B* **87**, 094420 (2013).
- [62] W.-J. Hu, F. Becca, A. Parola, and S. Sorella, Direct evidence for a gapless Z_2 spin liquid by frustrating Néel antiferromagnetism, *Phys. Rev. B* **88**, 060402(R) (2013).
- [63] F. Ferrari and F. Becca, Gapless spin liquid and valence-bond solid in the J_1 - J_2 Heisenberg model on the square lattice: Insights from singlet and triplet excitations, *Phys. Rev. B* **102**, 014417 (2020).
- [64] Y. Nomura and M. Imada, Dirac-type nodal spin liquid revealed by refined quantum many-body solver using neural-network wave function, correlation ratio, and level spectroscopy, *Phys. Rev. X* **11**, 031034 (2021).
- [65] V. G. Vaks, A. I. Larkin, S. A. Pikin, Thermodynamics of an ideal ferromagnetic substance, *Zh. Eksp. Teor. Fiz.* **53**, 281 (1967) [*Sov. Phys. JETP* **26**, 188 (1968)].
- [66] Y. A. Izyumov and Y. N. Skryabin, *Statistical Mechanics of Magnetically Ordered Systems*, (Springer, Berlin, 1988).
- [67] J. Halbinger, B. Schneider, and B. Sbierski, Spectral representation of Matsubara n -point functions: Exact kernel functions and applications, *SciPost Phys.* **15**, 183 (2023).
- [68] C. Honerkamp and M. Salmhofer, Temperature-flow renormalization group and the competition between superconductivity and ferromagnetism, *Phys. Rev. B* **64**, 184516 (2001).
- [69] Following Ref. [26] we normalize the scale-dependent dynamic spin susceptibility $G_\Lambda(\mathbf{k}, \omega)$ such that for free spins ($\Lambda = 0$), it is given by $G_0(\mathbf{k}, \omega) = \delta_{\omega,0} G_0(\mathbf{k}) = \delta_{\omega,0} / \Sigma_0 = \delta_{\omega,0} S(S+1)/3T$.
- [70] F. J. Dyson, General theory of spin-wave interactions, *Phys. Rev.* **102**, 1217 (1956).
- [71] S. Chakravarty, B. I. Halperin, and D. R. Nelson, Low-temperature behavior of two-dimensional quantum antiferromagnets, *Phys. Rev. Lett.* **60**, 1057 (1988).
- [72] S. Chakravarty, B. I. Halperin, and D. R. Nelson, Two-dimensional quantum Heisenberg antiferromagnet at low temperatures, *Phys. Rev. B* **39**, 2344 (1989).
- [73] P. Hasenfratz and F. Niedermayer, The exact correlation length of the antiferromagnetic $d = 2 + 1$ Heisenberg model at low temperatures, *Phys. Lett. B* **268**, 231 (1991).
- [74] P. Hasenfratz and F. Niedermayer, Finite size and temperature effects in the AF Heisenberg model, *Z. Phys. B* **92**, 91 (1993).
- [75] A. V. Chubukov, S. Sachdev, and J. Ye, Theory of two-dimensional quantum Heisenberg antiferromagnets with a nearly critical ground state, *Phys. Rev. B* **49**, 11919 (1994).
- [76] The expressions (22) and (24) for the scale-dependent contributions $V_\Lambda(\mathbf{k})$ and U_Λ to the static 4-point vertex are by construction consistent with the initial conditions at $\Lambda = 0$. The reason is that the we initialize the flow with the exact vertices of isolated spins that satisfy all sum rules automatically. To see this explicitly in Eq. (24) requires Taylor-expansion of numerator and denominator to first order in Λ and applying L'Hôpital's rule.
- [77] With the explicit expressions (29) for the contribution of the dynamic vertices, it is obvious that they do not contribute in the classical limit $S \rightarrow \infty$. After the appropriate rescaling $J_\Lambda(\mathbf{k})S^2 \rightarrow J_\Lambda(\mathbf{k})$, $\Sigma_\Lambda(\mathbf{k})S^2 \rightarrow \Sigma_\Lambda(\mathbf{k})$, $\Pi_\Lambda(K)S^{-2} \rightarrow \Pi_\Lambda(K)$, one finds that all dynamical diagrams contributing to the 2-point flow equations (24-26) are suppressed by a factor $1/S^2 \rightarrow 0$. Hence, only the static problem remains in this limit, and Eq. (24) for the quartic vertex simplifies to $U_\Lambda = 1/[T \int_q G_\Lambda^2(\mathbf{q})]$.
- [78] K. Tomita and H. Tomita, A dynamic approach to phase transition based on moments: Quasi-collective mode and the range of coherence, *Prog. Theor. Phys.* **45**, 1407 (1971).
- [79] N. D. Mermin and H. Wagner, Absence of ferromagnetism or antiferromagnetism in one- or two-dimensional isotropic Heisenberg models, *Phys. Rev. Lett.* **17**, 1133 (1966).
- [80] M. L. Baez and J. Reuther, Numerical treatment of spin systems with unrestricted spin length S : A functional renormalization group study, *Phys. Rev. B* **96**, 045144 (2017).
- [81] K. Fukui, Y. Kato, J. Nasu, and Y. Motome, Ground-state phase diagram of spin- S Kitaev-Heisenberg models, *Phys. Rev. B* **106**, 174416 (2022).